High-mobility pentacene thin-film transistor by using $La_xTa_{(1-x)}O_y$ as gate dielectric

Chuan Yu Han [a], Wing Man Tang [b], Cheung Hoi Leung[a], Chi Ming Che[c], Pui To Lai[a], *Senior Member, IEEE*

[a] Department of Electrical and Electronic, the University of Hong Kong, Hong Kong
[b] Department of Applied Physics, The Hong Kong Polytechnic University, Hong Kong
[c] Department of Chemistry, the University of Hong Kong, Hong Kong

Corresponding author: P. T. Lai
e-mail: laip@eee.hku.hk
Postal address: Room 505, CYC Building, Pokfulam Road, the University of Hong Kong, Hong Kong
Phone number: 852-28592691

Abstract

Pentacene organic thin-film transistors (OTFTs) using $La_xTa_{(1-x)}O_y$ as gate dielectric with different La contents (x = 0.227, 0.562, 0.764, 0.883) have been fabricated and compared with those using Ta oxide or La oxide. The OTFT with $La_{0.764}Ta_{0.236}O_y$ can achieve a carrier mobility of 1.21 $cm^2/V{\cdot}s$, which is about 40 times and two times higher than those of the devices using Ta oxide and La oxide, respectively. As supported by XPS, AFM and noise measurement, the reasons lie in that La incorporation can suppress the formation of oxygen vacancies in Ta oxide, and Ta content can alleviate the hygroscopicity of La oxide, resulting in more passivated and smoother dielectric surface and thus larger pentacene grains, which lead to higher carrier mobility.

Keywords Organic thin-film transistor, high-κ dielectric, La incorporation, TaLaO, oxygen vacancy

1 Introduction

Pentacene organic thin-film transistors (OTFTs) have recently attracted considerable attention because of their promising potential for radio-frequency identification tags (RFID)[1], sensors [2] and large-area flexible displays [3]. Although some OTFTs have shown good device performance comparable to amorphous silicon devices in terms of carrier mobility[1, 4, 5], the operating voltage of the OTFTs is still needed to be further reduced as many electronic devices are battery-powered at just a few volts. However, OTFTs fabricated with SiO_2 require a high operating voltage due to high threshold voltage (> 5 V), and thinning the dielectric film to reduce the operating voltage inevitably enlarges the leakage current. Therefore, a dielectric material with high dielectric constant (i.e. high-κ) is necessary to be employed in order to lower the threshold voltage. Various high-κ materials have been reported for pentacene OTFT and its carrier mobility varies from 2×10^{-2} to 1.4 $cm^2/V\cdot s$ [6-8]. Among them, the mobility of pentacene OTFT on pure Ta_2O_5 varied from 0.03 to 0.32 $cm^2/V\cdot s$, depending on the growth method, surface modification and thickness of the Ta_2O_5 film [9-11], while that on La_2O_3 was reported to reach 0.02 $cm^2/ V\cdot s$ [12].The performance of the OTFT highly depends on the quality of its high-κ gate dielectric, such as surface roughness and trap density. Recently, it has been reported that the addition of La could suppress the oxygen vacancy of the Hf-based high-κ materials[13, 14], and OTFTs using HfLaO as gate dielectric have achieved high performance, such as high carrier mobility, low threshold voltage and small sub-threshold swing (SS) [15].

Ta_2O_5 has high κ value (~ 26), but it has small band gap (~ 4.4 eV) and suffers from a high concentration of oxygen vacancies, whose gap states lead to charge trapping[16, 17]. On the other hand, La_2O_3 with larger band gap (~ 6 eV) is very hygroscopic and unstable in air, forming hydroxide[18]. In this study, $La_xTa_{(1-x)}O_y$ films with different La contents are prepared by RF sputtering and proposed as the gate dielectric of pentacene OTFT in an attempt to combine the advantages of La_2O_3 and Ta_2O_5 while suppressing their undesirable properties. By using $La_xTa_{(1-x)}O_y$ with proper La content (76.4% La) as gate dielectric, high-performance OTFT with high carrier mobility and low threshold voltage can be obtained.

2 Experimental details

Initially, silicon wafers (n-type, <100>, resistivity of 0.5 ~ 1 Ω·cm) were cleaned according to the standard RCA method and dipped in 2 % hydrofluoric acid to remove the native oxide. Then, $La_xTa_{(1-x)}O_y$ (with x = 0, 0.227, 0.562, 0.764, 0.883, and 1) films were deposited by sputtering in Ar/O_2 (24:6 sccm) ambient. A radio-frequency sputterer (Denton Vacuum LLC Discovery 635) as well as Ta and La_2O_3 targets were employed to prepare the $La_xTa_{(1-x)}O_y$ films at different sputtering powers. After that, the samples were annealed in O_2 at 400 ºC for 30 min, with a flow rate of 1000 sccm. Next, 30-nm pentacene (99 %, purchased from Sigma-Aldrich without purification) was evaporated on the dielectrics by an evaporator (Edwards Auto 306) in high vacuum (4×10^{-6} torr) at a deposition rate of 1.3 nm/min, monitored by a quartz-crystal oscillator. Lastly, gold was deposited on the pentacene film by evaporation through a shadow mask to form the drain and source electrodes of the OTFTs. The width and length of the channel on the shadow mask were 200 μm and 30 μm, respectively.

The electrical characteristics and low-frequency noise (LFN) of the transistors were measured by HP 4145B semiconductor parameter analyzer, Berkeley Technology Associates Model 9603 FET noise analyzer and HP 35665A dynamic signal analyzer. Al/high-κ dielectric/heavily-doped Si MOS structure was also fabricated by lithography for measuring the dielectric capacitance with HP 4284A precision LCR meter. All the measurements were conducted at room temperature, in air, and under shielded environment. The thickness of the dielectric films was measured by a Wvase 32 ellipsometer. A Veeco multi-mode scanning probe microscope was employed to record the surface morphologies of the dielectrics and pentacene films. The physical characteristics of the high-κ dielectric films were characterized by X-ray photoelectron spectroscopy (XPS). The binding energies were corrected for the sample charging effect with reference to the C 1s peak at 284.5 eV.

3 Results and discussions

3.1 XPS of the gate dielectrics

Fig. 1 shows the XPS spectrum of O 1*s* for $La_xTa_{(1-x)}O_y$ films with different La contents. It is clear that when the La content increases, more La-O-H bonds are formed in the $La_xTa_{(1-x)}O_y$ film due to the hygroscopicity of the La oxide. Fig. 2(a) shows that the binding energy of Ta 4*f* is shifted to lower value with the increase of the La content, which should be caused by the La incorporation suppressing the oxygen vacancy in the Ta oxide. It is widely accepted that the oxygen vacancy is positively charged and generates an electric field [19-21], thus leading to binding-energy shift [22]. The binding energy increases when an atom is placed near a positive charge [22]. Hence, reducing oxygen vacancies in the Ta oxide and thus the positive charges around the Ta atoms via the addition of La can result in a shift of Ta 4*f* peak toward lower binding energy. On the other hand, incorporating Ta into La oxide can generate more positive oxygen vacancies, resulting in higher binding energy for La 3*d*. In Fig. 2(b), the XPS spectra of La 3*d* in $La_xTa_{(1-x)}O_y$ with 1-x = 0.236, 0.438 and 0.773 are shifted to higher binding energy with the increase of Ta content. However, by comparing the spectra of La 3*d* for the $La_xTa_{(1-x)}O_y$ oxides with 1-x = 0.116 and 0.236, it is found that the binding-energy shift of La 3*d* behaves differently at low Ta content. With increasing Ta content and decreasing the amount of La,

the formation of La-O-H bond due to water absorption is suppressed, causing a shift of the La 3*d* peak to lower binding energy as the La-O-H bond has higher binding energy than the La-O bond [23]. In addition, it has been reported that La incorporation into Hf-based high-κ dielectrics can suppress the formation of oxygen vacancy due to the decrease of local dielectric constant around the La atom[13]. It is highly possible that the same mechanism can be applied to the La-doped Ta oxide because La_2O_3 also has lower κ value than Ta_2O_5.

3.2 AFM images of the pentacene films

Fig. 3 shows the AFM image of 30-nm pentacene film deposited on $La_xTa_{(1-x)}O_y$ film with different La contents. The pentacene grain size first increases with the La content, and then decreases slightly after the La content reaches x = 0.764. Sample D has the most uniform-sized and largest grains among the samples. The pentacene grain size on the La-doped Ta oxide or La oxide (see Fig.3(b)-(f)) is much larger than that on the Ta oxide (see Fig. 3 (a)). The main reason should be that adding La into Ta oxide reduces its traps caused by the oxygen vacancies, which can act as nucleation sites for the growth of pentacene grains on the oxide surface [24-27]. With fewer nucleation sites on the surfaces of the La-doped Ta oxide and La_2O_3, larger pentacene grains can be formed on these oxide films.

3.3 Electrical properties of the OTFTs

The sub-threshold swing (SS) is defined as

$$SS = \frac{dV_G}{d(\log I_D)}, \tag{1}$$

where I_D is the drain current, and V_G the gate voltage.

Assuming that both the density of deep bulk trap and density of deep interface trap are independent of trap energy, the sub-threshold swing can be written as [28]

$$SS = \frac{kT \ln 10}{e}\left[1 + \frac{e}{C_{ox}} N_t\right]. \tag{2}$$

where N_t is the density of deep bulk trap and interface trap per unit area and unit energy, C_{ox} the insulator capacitance per unit area, k the Boltzmann's constant, e the electron charge and T the temperature in Kelvin. Therefore, the trap density can be extracted from measured SS value using equation (2). The transfer characteristics of the OTFTs are shown in Fig. 4. The key parameters of the OTFTs are extracted and summarized in Table 1.

The sample D exhibits the highest carrier mobility of 1.21 cm/V·s, which is about forty times and two times higher than the devices using Ta oxide and La oxide respectively. The carrier mobility first increases with the La content and then decreases when the La content reaches x = 0.764. The highest carrier mobility of the sample D (with x = 0.764) should be attributed to its most uniform-sized and largest pentacene grains (see Fig. 3), resulted from its smoother dielectric surface (smaller RMS roughness in Table 1) and best suppression of oxygen vacancy in the dielectric (smallest SS in Table 1) induced by the La incorporation. However, La easily absorbs water moisture and then roughens the surface of the gate dielectric. While the samples B, C and D basically have the same RMS roughness, the samples E and F have much rougher oxide surface and thus stronger carrier scattering at the pentacene/gate-oxide interface, thereby lower carrier mobility.

It is reported that the carrier mobility is dependent on the thickness of the gate dielectric[29]. Therefore, in order to better compare the performance of the devices with different gate-dielectric thicknesses, μC_{ox} which is directly related to $2I_D L / W(V_G - V_T)^2$, is employed to characterize the devices with threshold voltage of V_T. As listed in Table 1, μC_{ox} of the samples D and E is much better than those of the samples A and F. This reveals that $La_xTa_{(1-x)}O_y$ with x = 0.764 or 0.883 can greatly improve the gate control property of the device.

All the OTFTs show good field-effect property and saturation behavior, and can operate at a very low voltage of less than 5 V as shown in Fig. 5. Among all the studied devices, sample D has the largest drain current at V_G = -5 V because of its highest carrier mobility.

3.4 LFN of the OTFTs

The LFN of OTFT is very sensitive to carrier-number fluctuation in the conduction channel and therefore is used to study the traps located at the interface between pentacene and gate dielectric [30]. The LFN spectrum of the devices in Fig. 6 reveals that La incorporation in Ta oxide can reduce the LFN and thus the traps. Moreover, with optimal La incorporation, the sample D exhibits the lowest LFN, further supporting its lowest trap density among the devices.

4 Conclusion

In sum, pentacene OTFTs using $La_xTa_{(1-x)}O_y$ as gate dielectric with different La contents (x = 0.227, 0.562, 0.764, 0.883) have been fabricated and compared with their counterparts based on Ta oxide or La oxide. The dielectric films were deposited using co-sputtering of Ta and La_2O_3 targets in Ar/O_2 ambient by varying the sputtering powers of the targets. The binding-energy shift of the XPS spectra reveals that the La incorporation can suppress the formation of oxygen vacancies in Ta oxide, thus reducing the nucleation sites at the oxide surface to obtain larger pentacene grains and hence less grain-boundary-induced carrier scattering in the conduction channel. On the other hand, the incorporation of Ta into La oxide can alleviate the hygroscopicity of La oxide, resulting in a smoother dielectric surface, which can also give rise to larger pentacene grains and less surface-roughness scattering. Among the devices, the OTFT with $La_{0.764}Ta_{0.236}O_y$ as gate dielectric can achieve the highest carrier mobility of 1.21 $cm^2/V{\cdot}s$, which is about 40 times and two times higher than the devices using Ta oxide and La oxide respectively. AFM confirms that largest grains are formed on this oxide film with a smooth surface. The smallest SS and lowest LFN achieved by this OTFT further support that this device has the best interface quality between the pentacene film and the oxide film.

Acknowledgements

This work is supported by the URC for Seed Fund for Strategic Research Theme of HKU on New Materials, and the University Development Fund (Nanotechnology Research Institute, 00600009) of the University of Hong Kong. The authors would like to acknowledge Dickey Ma for his help.

References

[1] P.F. Baude, D.A. Ender, M.A. Haase, T.W. Kelley, D.V. Muyres, S.D. Theiss, Pentacene-based radio-frequency identification circuitry, Appl Phys Lett, 82 (2003) 3964-3966.

[2] H.W. Zan, W.W. Tsai, Y.R. Lo, Y.M. Wu, Y.S. Yang, Pentacene-Based Organic Thin Film Transistors for Ammonia Sensing, Ieee Sens J, 12 (2012) 594-601.

[3] C.D. Sheraw, L. Zhou, J.R. Huang, D.J. Gundlach, T.N. Jackson, M.G. Kane, I.G. Hill, M.S. Hammond, J. Campi, B.K. Greening, J. Francl, J. West, Organic thin-film transistor-driven polymer-dispersed liquid crystal displays on flexible polymeric substrates, Appl Phys Lett, 80 (2002) 1088-1090.

[4] M.H. Zhang, S.P. Tiwari, B. Kippelen, Pentacene organic field-effect transistors with polymeric dielectric interfaces: Performance and stability, Org Electron, 10 (2009) 1133-1140.

[5] M. Devynck, P. Tardy, G. Wantz, Y. Nicolas, L. Vellutini, C. Labrugere, L. Hirsch, Cumulative effects of electrode and dielectric surface modifications on pentacene-based transistors, Appl Phys Lett, 100 (2012) 053308.

[6] M. Shtein, J. Mapel, J.B. Benziger, S.R. Forrest, Effects of film morphology and gate dielectric surface preparation on the electrical characteristics of organic-vapor-phase-deposited pentacene thin-film transistors, Appl Phys Lett, 81 (2002) 268-270.

[7] R.E.I. Schropp, B. Stannowski, J.K. Rath, New challenges in thin film transistor (TFT) research, J Non-Cryst Solids, 299 (2002) 1304-1310.

[8] R.P. Ortiz, A. Facchetti, T.J. Marks, High-k organic, inorganic, and hybrid dielectrics for low-voltage organic field-effect transistors, Chem Rev, 110 (2010) 205-239.

[9] A.L. Deman, J. Tardy, PMMA-Ta2O5 bilayer gate dielectric for low operating voltage organic FETs, Org Electron, 6 (2005) 78-84.

[10] A.L. Deman, M. Erouel, D. Lallemand, M. Phaner-Goutorbe, P. Lang, J. Tardy, Growth related properties of pentacene thin film transistors with different gate dielectrics, J Non-Cryst Solids, 354 (2008) 1598-1607.

[11] Y. Zhao, G.F. Dong, L.D. Wang, Y. Qiu, Improved photostability of organic thin film transistors with tantalum oxide/poly(4-vinylphenol) double gate insulators, Appl Phys Lett, 90 (2007) 252110.

[12] P.K. Saikia, U.J. Mahanta, P. Saikia, B. Baishya, R. Sarma, D. Saikia, Low threshold voltage pentacene OTFTs with La_2O_3 gate insulating layer using TSD, Chiang Mai J Sci, 39 (2012) 263-269.

[13] N. Umezawa, K. Shiraishi, S. Sugino, A. Tachibana, K. Ohmori, K. Kakushima, H. Iwai, T. Chikyow, T. Ohno, Y. Nara, K. Yamada, Suppression of oxygen vacancy formation in Hf-based high-k dielectrics by lanthanum incorporation, Appl Phys Lett, 91 (2007) 132904.

[14] D. Liu, J. Robertson, Passivation of oxygen vacancy states and suppression of Fermi pinning in HfO_2 by La addition, Appl Phys Lett, 94 (2009) 042904.

[15] M.F. Chang, P.T. Lee, S.P. McAlister, A.S. Chin, Small-subthreshold-swing and low-voltage fexible organic thin-film transistors which use HfLaO as the gate dielectric, IEEE Electr Device Lett, 30 (2009) 133-135.

[16] R. Ramprasad, First principles study of oxygen vacancy defects in tantalum pentoxide, J Appl Phys, 94 (2003) 5609.

[17] H. Sawada, K. Kawakami, Electronic structure of oxygen vacancy in Ta_2O_5, J Appl Phys, 86 (1999) 956.

[18] Y. Zhao, M. Toyama, K. Kita, K. Kyuno, A. Toriumi, Moisture-absorption-induced permittivity deterioration and surface roughness enhancement of lanthanum oxide films on silicon, Appl Phys Lett, 88 (2006) 072904.

[19] T.L. Duan, H.Y. Yu, L. Wu, Z.R. Wang, Y.L. Foo, J.S. Pan, Investigation of HfO_2 high-k dielectrics electronic structure on SiO_2/Si substrate by x-ray photoelectron spectroscopy, Appl Phys Lett, 99 (2011) 012902.

[20] S. Guha, V. Narayanan, Oxygen vacancies in high dielectric constant oxide-semiconductor films, Phys Rev Lett, 98 (2007) 196101.

[21] K. Xiong, J. Robertson, M.C. Gibson, S.J. Clark, Defect energy levels in HfO2 high-dielectric-constant gate oxide, Appl Phys Lett, 87 (2005) 183505.

[22] P.S. Bagus, F. Illas, G. Pacchioni, F. Parmigiani, Mechanisms responsible for chemical shifts of core-level binding energies and their relationship to chemical bonding, J Electron Spectrosc, 100 (1999) 215-236.

[23] M.F. Sunding, K. Hadidi, S. Diplas, O.M. Lovvik, T.E. Norby, A.E. Gunnaes, XPS characterisation of in situ treated lanthanum oxide and hydroxide using tailored charge referencing and peak fitting procedures, J Electron Spectrosc, 184 (2011) 399-409.

[24] M. Voigt, J. Pflaum, M. Sokolowski, Growth morphologies and charge carrier mobilities of pentacene organic field effect transistors with rf sputtered aluminium oxide gate insulators on ITO glass, Physica Status Solidi (A), 205 (2008) 449-460.

[25] M.C. Kwan, K.H. Cheng, P.T. Lai, C.M. Che, Improved carrier mobility for pentacene TFT by NH_3 annealing of gate dielectric, Solid State Electron, 51 (2007) 77-80.

[26] S. Godlewski, M. Szymonski, Adsorption and self-assembly of large polycyclic molecules on the surfaces of TiO_2 single crystals, Int J Mol Sci, 14 (2013) 2946-2966.

[27] C. Sanchez-Sanchez, G. Bavdek, D. Cvetko, M.F. Lopez, J.A. Martin-Gago, L. Floreano, Planar growth of pentacene on the dielectric TiO_2(110) surface, The Journal of Physical Chemistry C, 115 (2011) 4664-4672.

[28] W.L. Kalb, B. Batlogg, Calculating the trap density of states in organic field-effect transistors from experiment: A comparison of different methods, Phys Rev B, 81 (2010) 035327.

[29] Z.R. Wang, J.Z. Xin, X.C. Ren, X.L. Wang, C.W. Leung, S.Q. Shi, A. Ruotolo, P.K.L. Chan, Low power flexible organic thin film transistors with amorphous Ba0.7Sr0.3TiO3 gate dielectric grown by pulsed laser deposition at low temperature, Org Electron, 13 (2012) 1223-1228.

[30] L. Ke, S. Bin Dolmanan, L. Shen, C. Vijila, S.J. Chua, R.Q. Png, P.J. Chia, L.L. Chua, P.K.H. Ho, Low frequency noise analysis on organic thin film transistors, J Appl Phys, 104 (2008) 124502.

Figure Caption

Fig. 1 XPS spectrum of O 1s for $La_xTa_{(1-x)}O_y$ with x = 0.227 (a), 0.562 (b), 0.764 (c), and 0.883 (d).
Fig. 2 XPS spectra of Ta 4*f* (a) and La 3*d* (b).
Fig. 3 AFM image ($2\times2\mu m^2$) of pentacene film (30 nm) on $La_xTa_{(1-x)}O_y$ with x = (a) 0 for sample A, (b) 0.227 for sample B, (c) 0.562 for sample C, (d) 0.764 for sample D, (e) 0.883 for sample E and (f) 1 for sample F. The average grain size for samples A, B, C, D, E and F is 1.14×10^4 nm^2, 2.14×10^4 nm^2, 4.21×10^4 nm^2, 5.60×10^4 nm^2, 5.01×10^4 nm^2, 4.34×10^4 nm^2, respectively.
Fig. 4 Transfer characteristics of the OTFTs with different La contents.
Fig. 5 Output characteristics of the OTFTs with different La contents.
Fig. 6 Low-frequency noise spectrum of the OTFTs with different La contents.

Fig. 1

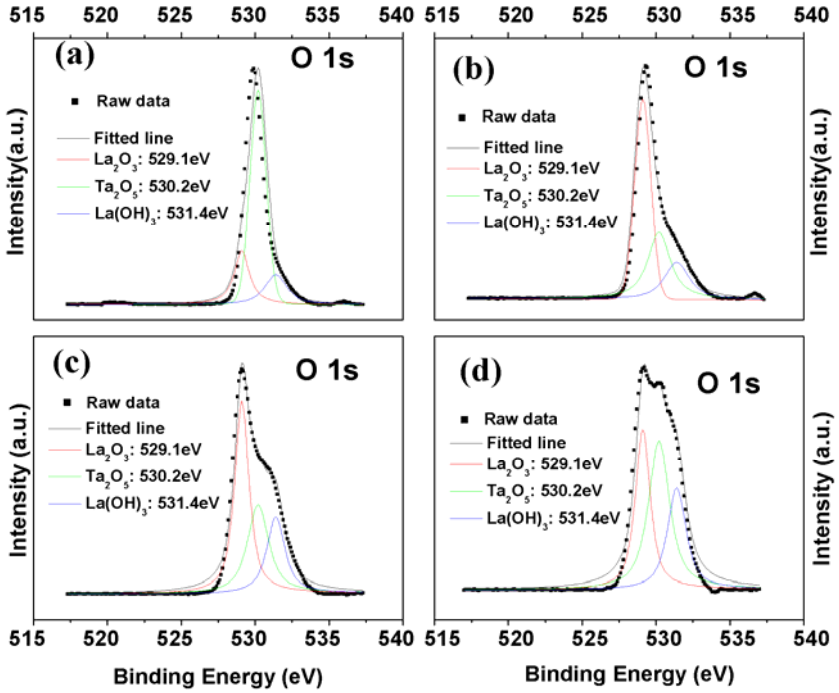
(a)
O 1s
Raw data
Fitted line
La2O3: 529.1eV
Ta2O5: 530.2eV
La(OH)3: 531.4eV
Intensity(a.u.)
(b)
O 1s
Raw data
Fitted line
La2O3: 529.1eV
Ta2O5: 530.2eV
La(OH)3: 531.4eV
Intensity(a.u.)
(c)
O 1s
Raw data
Fitted line
La2O3: 529.1eV
Ta2O5: 530.2eV
La(OH)3: 531.4eV
Intensity (a.u.)
(d)
O 1s
Raw data
Fitted line
La2O3: 529.1eV
Ta2O5: 530.2eV
La(OH)3: 531.4eV
Intensity (a.u.)
515 520 525 530 535 540
Binding Energy (eV)

Fig. 2

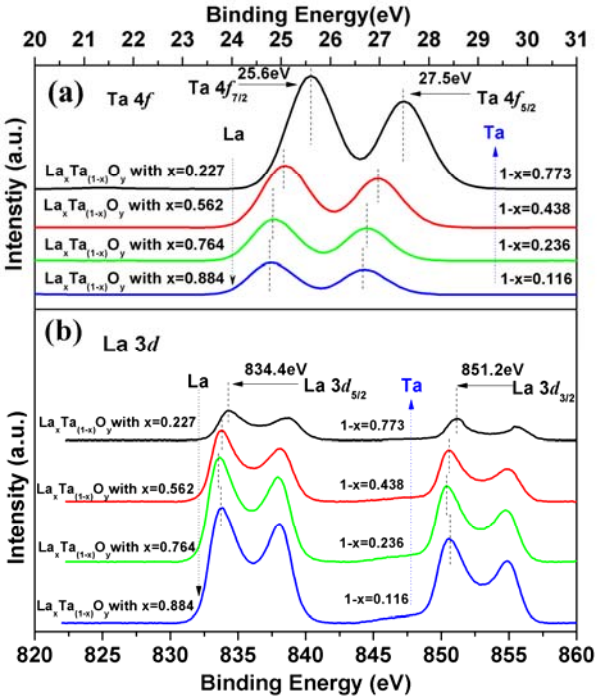
Binding Energy(eV)
20 21 22 23 24 25 26 27 28 29 30 31
(a) Ta 4f
Ta 4f7/2
25.6eV
27.5eV
Ta 4f5/2
La
Ta
LaxTa(1-x)Oy with x=0.227
1-x=0.773
LaxTa(1-x)Oy with x=0.562
1-x=0.438
LaxTa(1-x)Oy with x=0.764
1-x=0.236
LaxTa(1-x)Oy with x=0.884
1-x=0.116
Intenstiy (a.u.)
(b) La 3d
La
834.4eV
La 3d5/2
Ta
851.2eV
La 3d3/2
LaxTa(1-x)Oy with x=0.227
1-x=0.773
LaxTa(1-x)Oy with x=0.562
1-x=0.438
LaxTa(1-x)Oy with x=0.764
1-x=0.236
LaxTa(1-x)Oy with x=0.884
1-x=0.116
Intensity (a.u.)
820 825 830 835 840 845 850 855 860
Binding Energy (eV)

Fig. 3

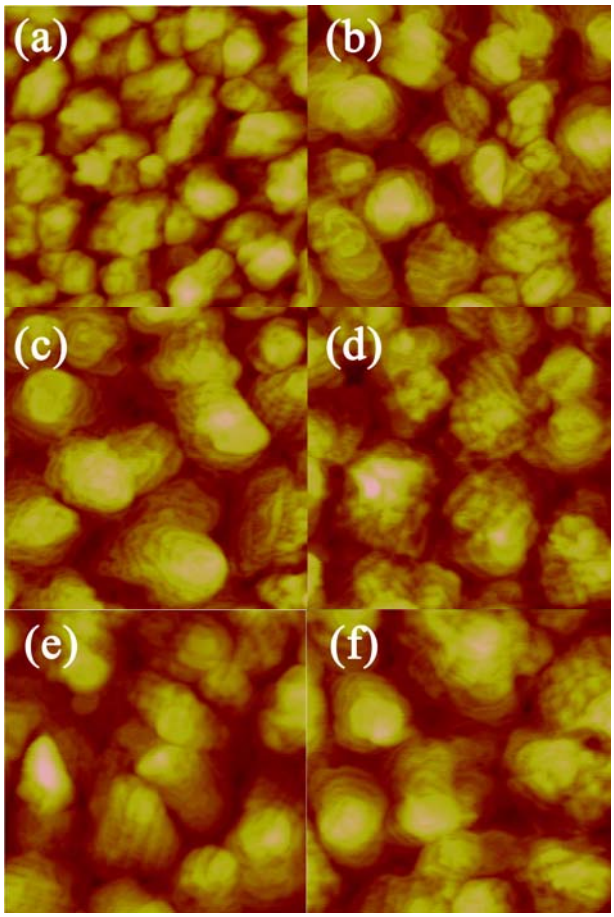
(a)
(b)
(c)
(d)
(e)
(f)

Fig. 4

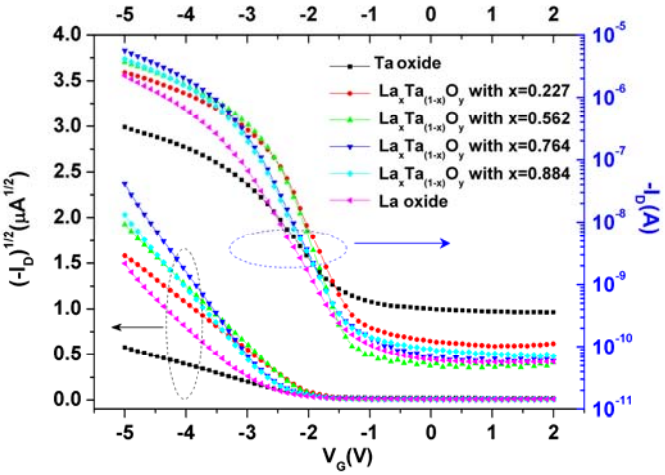
Ta oxide
La$_x$Ta$_{(1-x)}$O$_y$ with x=0.227
La$_x$Ta$_{(1-x)}$O$_y$ with x=0.562
La$_x$Ta$_{(1-x)}$O$_y$ with x=0.764
La$_x$Ta$_{(1-x)}$O$_y$ with x=0.884
La oxide
$(-I_D)^{1/2}(\mu A^{1/2})$
$-I_D(A)$
$V_G(V)$

Fig. 5

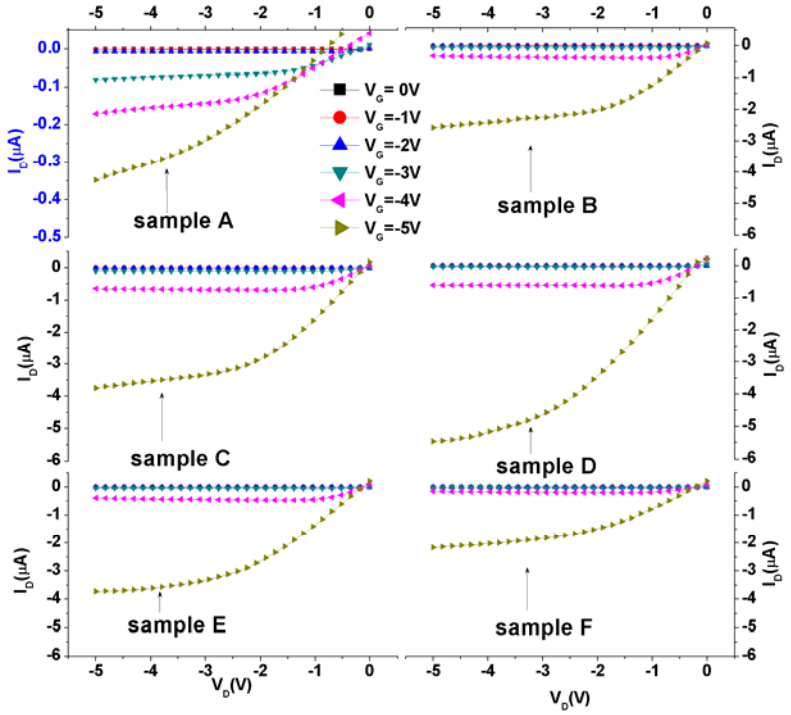
V_G= 0V
V_G=-1V
V_G=-2V
V_G=-3V
V_G=-4V
V_G=-5V
sample A
sample B
sample C
sample D
sample E
sample F
I_D(μA)
V_D(V)

Fig. 6

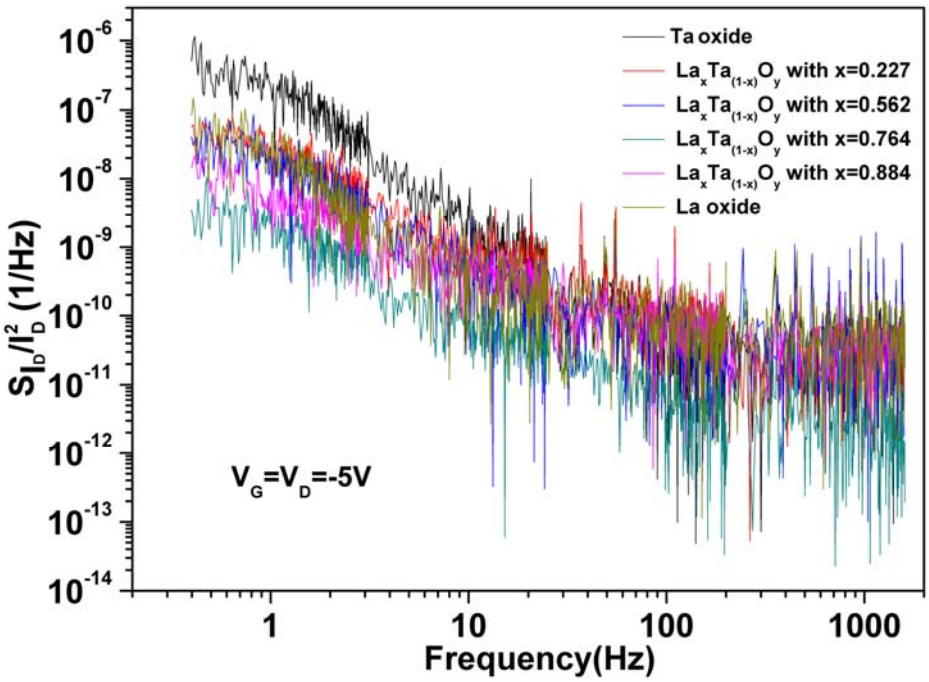
Ta oxide
La_xTa_(1-x)O_y with x=0.227
La_xTa_(1-x)O_y with x=0.562
La_xTa_(1-x)O_y with x=0.764
La_xTa_(1-x)O_y with x=0.884
La oxide
V_G=V_D=-5V
S_ID/I_D^2 (1/Hz)
Frequency(Hz)